Ribosomal protein RPL26 is the principal target of UFMylation

Christopher P. Walczak[a], Dara E. Leto[a], Lichao Zhang[b], Celeste Riepe[c], Ryan Y. Muller[c], Paul A. DaRosa[a], Nicholas T. Ingolia[c], Joshua E. Elias[b], and Ron R. Kopito[a,1]

[a]Department of Biology, Stanford University, Stanford, CA 94305; [b]Department of Chemical and Systems Biology, Stanford University, Stanford, CA 94305; and [c]Department of Molecular and Cell Biology, University of California, Berkeley, CA 94720

Edited by Brenda A. Schulman, Max Planck Institute of Biochemistry, and approved December 10, 2018 (received for review September 19, 2018)

Ubiquitin fold modifier 1 (UFM1) is a small, metazoan-specific, ubiquitin-like protein modifier that is essential for embryonic development. Although loss-of-function mutations in UFM1 conjugation are linked to endoplasmic reticulum (ER) stress, neither the biological function nor the relevant cellular targets of this protein modifier are known. Here, we show that a largely uncharacterized ribosomal protein, RPL26, is the principal target of UFM1 conjugation. RPL26 UFMylation and de-UFMylation is catalyzed by enzyme complexes tethered to the cytoplasmic surface of the ER and UFMylated RPL26 is highly enriched on ER membrane-bound ribosomes and polysomes. Biochemical analysis and structural modeling establish that UFMylated RPL26 and the UFMylation machinery are in close proximity to the SEC61 translocon, suggesting that this modification plays a direct role in cotranslational protein translocation into the ER. These data suggest that UFMylation is a ribosomal modification specialized to facilitate metazoan-specific protein biogenesis at the ER.

UFMylation | RPL26 | UFM1 | endoplasmic reticulum

Ubiquitin fold modifier 1 (UFM1) is an 85-amino acid ubiquitin-like protein modifier (UBL) that is ubiquitously expressed in metazoans but absent from fungi (1) and is essential for brain and hematopoietic development (2–4). Like ubiquitin and other UBLs, UFM1 is covalently ligated to lysine residues on target proteins by a three-step cascade catalyzed by E1, E2, and E3 enzymes, encoded by *UBA5*, *UFC1*, and *UFL1* genes, respectively (1, 5) (Fig. 1*A*). UFM1 is cleaved from its targets by the UFM1-specific thiol protease, UFSP2 (5–7). Although the basic chemistry of UFM1 conjugation is well understood, its physiological function is not. Homozygous disruption of the UFM1 pathway in mice causes midgestation embryonic lethality associated with impaired hematopoiesis (2, 8–10). In humans, hypomorphic loss-of-function alleles of genes that code for UFM1, UBA5, or UFPS2 are linked to diverse pathologies, including leukodystrophy (3), epileptic encephalopathy (11), spinocerebellar ataxia (12), and skeletal abnormalities (13–15), revealing an essential role for UFMylation in multiple organ systems. Although several cellular proteins have been reported to be UFMylation targets (5, 7, 16–18), none of these have been demonstrated to form covalent adducts with UFM1 under physiological conditions and none have been plausibly linked to the cellular or organismal pathophysiologies associated with loss-of-function UFMylation mutants in humans or experimental animals.

UFMylation is intimately linked to the secretory pathway. The UFM1-specific ligase, UFL1, is recruited to the cytosolic face of the endoplasmic reticulum (ER) membrane, likely through its stable association with the ER resident transmembrane protein, DDRGK1 (19). Moreover, UFMylation genes are transcriptional targets of the unfolded protein response (UPR) and the *UFM1* promoter contains a putative binding site for the ER stress-responsive transcriptional activator XBP1 (20). Targeted disruption of genes encoding UFM1 or UFM1 conjugation machinery weakly activates an ER stress response in a subset of cell types in culture (21–23) and enhances ER stress-induced apoptosis in pancreatic beta cells (24). Although the UFMylation pathway is not essential for viability of cells in culture, the impaired hematopoeisis observed in embryonic lethal mouse knockouts of *Uba5*, *Ufl1*, or *Ddrgk1* (8–10), and cardiomyopathy ensuing from heart-specific disruption of *Ufl1* (25), is accompanied by elevated markers of ER stress. Despite this circumstantial evidence linking the UFMylation system to the ER, reported UFMylation targets expressed at endogenous levels are neither physically nor physiologically associated with the ER. Unambiguous identification of covalent, physiological UFM1 targets holds the key to elucidating the biological function of this essential, metazoan-specific protein modification.

Here we combine genetic disruption of UFMylation and de-UFMylation with affinity capture LC-MS/MS to show that the conserved ribosomal protein RPL26 (uL24) is the principal target of UFMylation in human cells. Our data show that ribosome-bound RPL26 is covalently UFMylated and de-UFMylated by enzymes tethered to the ER membrane. Inhibition of RPL26 UFMylation or de-UFMylation leads to impaired ER protein homeostasis. These findings suggest that covalent modification of RPL26 with UFM1 plays a key role in protein biogenesis in the early secretory pathway.

Results

Loss of UFMylation or De-UFMylation Impairs ER-Associated Protein Degradation. We identified the entire suite of genes encoding the UFM1 system, including UFM1 itself and all known conjugation and deconjugation enzymes, in a genome-wide CRISPR/Cas9-mediated gene knockout analysis of substrate-selective ER-associated protein degradation (ERAD) in human K562 erythroleukemia cells (26) (Fig. 1*B*). ERAD is a quality control process by which folding- or assembly- defective proteins are targeted for proteasome-mediated

Significance

Ubiquitin fold modifier 1 (UFM1) is a ubiquitin-like post-translational modifier that is essential for tissue development in metazoans. Genetic ablation of UFM1 or the genes that encode the enzymes that conjugate UFM1 to protein targets causes endoplasmic reticulum (ER) stress, suggesting a role for this modification in ER protein homeostasis. Here, we show that RPL26, a largely uncharacterized ribosomal protein, is the primary cellular target of UFMylation. Ribosomal RPL26 is subject to a dynamic cycle of UFMylation and de-UFMylation, catalyzed by enzymes that are tethered to the cytoplasmic surface of the ER. UFMylated RPL26 and the UFMylation machinery are in close proximity to the SEC61 translocon, suggesting a role for UFMylation in protein biogenesis at the ER.

Author contributions: C.P.W., D.E.L., C.R., and R.R.K. designed research; C.P.W., D.E.L., L.Z., C.R., R.Y.M., and P.A.D. performed research; C.P.W. and D.E.L. contributed new reagents/analytic tools; C.P.W., D.E.L., L.Z., C.R., P.A.D., N.T.I., J.E.E., and R.R.K. analyzed data; and C.P.W., D.E.L., and R.R.K. wrote the paper.

The authors declare no conflict of interest.

This article is a PNAS Direct Submission.

[1]To whom correspondence should be addressed. Email: kopito@stanford.edu.

This article contains supporting information online at www.pnas.org/lookup/suppl/doi:10.1073/pnas.1816202116/-/DCSupplemental.

Published online January 9, 2019.

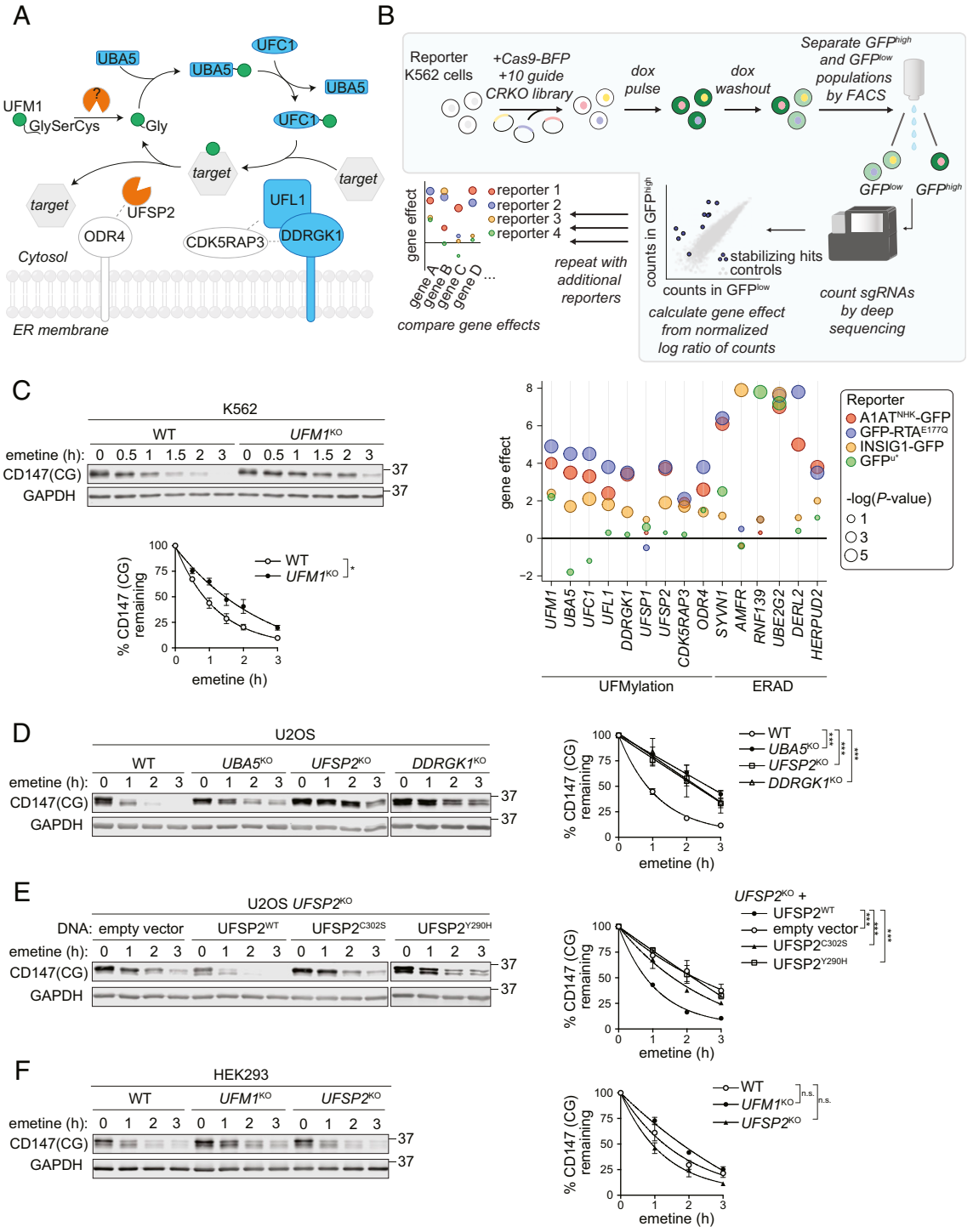

Fig. 1. Loss of UFMylation or de-UFMylation impairs ERAD. (*A*) The UFMylation system shown in relation to the ER membrane bilayer. Known UFM1 conjugation or deconjugation machinery is rendered in blue and orange, respectively. Interacting partners of unknown function are shown in white with interactions denoted by dashed lines. (*B*) Identification of the UFMylation pathway from functional genomic analysis of substrate-selective ERAD. (*Top*) Forward genetic screening pipeline. Four independent genome-wide screens were iteratively conducted with the indicated GFP-tagged reporters and the data combined into a "gene effect" metric. Complete details can be found in ref. 26. (*Bottom*) Bubble plot of gene effects for UFM1-related genes and a reference set of ERAD genes. Data are from table S1 in ref. 26. Each of the four ERAD reporters is represented by a different colored bubble; the diameter indicates the −log *P* value. *SYVN1* encodes HRD1, *AMFR* encodes GP78, and *RNF139* encodes TRC8. (*C*) *UFM1* knockout impairs turnover of CD147(CG) in K562 cells. (*Top*) Cells were treated with the protein synthesis inhibitor, emetine, for the indicated times before lysis. Lysates were analyzed by immunoblotting with the indicated antibodies. (*Bottom*) Quantification of emetine chases represented by mean ± SEM; $n = 3$. $^{*}P < 0.05$ obtained by Student's *t* test. (*D*) Turnover of CD147(CG) in U2OS cells is impaired by loss of UFMylation or de-UFMylation machinery. Emetine chases were performed and quantified as in *C*. $n = 8$ for wild type; $n = 4$ for *UBA5*^{KO}, $n = 5$ for *UFSP2*^{KO}, $n = 4$ for *DDRGK1*^{KO}. $^{***}P < 0.001$ obtained by Student's *t* test. (*E*) Turnover of CD147(CG) is impaired in U2OS cells expressing catalytically inactive UFSP2. Emetine chases were performed and quantified as in *C*; $n = 3$. $^{***}P < 0.001$ obtained by Student's *t* test. (*F*) Turnover of CD147(CG) in HEK293 cells is not affected by loss of UFMylation or de-UFMylation. Emetine chases were performed and quantified as in *C*; $n = 3$. n.s., statistically not significant, $P > 0.05$ obtained by Student's *t* test.

degradation by ubiquitin conjugating machinery embedded in the ER membrane (27). Knockout of genes required for UFM1 conjugation (*UFM1*, *UBA5*, *UFC1*, *UFL1*, and *DDRGK1*) or deconjugation (*UFSP2*) stabilized two luminal clients of the HRD1 ubiquitin ligase/dislocase (encoded by *SYVN1*) (28), α-1 antitrypsin null Hong Kong variant (A1AT^{NHK}-GFP) and a catalytically attenuated ricin A chain variant (GFP-RTA^{E177Q}). Deletion of *UFSP1*, which in humans encodes a catalytically inactive homolog of the UFM1 deconjugase, had no effect on ERAD. The cytoplasmic UPS reporter, GFP$^{ u}$*, which is ubiquitylated by a different ER-embedded ubiquitin ligase, TRC8 (encoded by *RNF139*) (26, 29), was not affected by loss of UFMylation or de-UFMylation. Disruption of UFM1-related genes also led to modest stabilization of INSIG1-GFP, a hydrophobic integral membrane client of the GP78 ubiquitin ligase (encoded by *AMFR*) (30). Stabilization of A1AT^{NHK}-GFP and GFP-RTA^{E177Q} in response to acute disruption of UFMylation was validated by translational shutoff kinetic analysis in K562 cells harboring single gene knockouts (*SI Appendix*, Fig. S1 *A* and *B*). The effects of disrupting UFMylation genes on ERAD were highly significant ($P < 0.001$), but were quantitatively modest (gene effect 1.8–4.2) compared with knocking out genes encoding core ERAD ubiquitin ligases (gene effect >6) that physically engage substrates (Fig. 1*B*). The gene effect is a phenotype estimate calculated from the median-normalized $\log_2$ ratio of sgRNA counts between GFP^{high} and GFP^{low} cells and is highly correlated with actual reporter turnover rates (26). This modest phenotype may indicate either a direct role of UFMylation in HRD1-dependent ERAD that is compensated by genetic redundancy or an indirect effect in which disruption of UFMylation causes misfolded proteins to accumulate in the ER, where they could compete with our reporters for access to limiting ERAD machinery. While either possibility is consistent with the observation of partially penetrant modest induction of ER stress in *UFM1*^{KO} cells (21–23), our finding that impaired UFMylation leads to stabilization of *both* HRD1 and GP78 clients supports the latter model.

To further distinguish between these two mechanisms we evaluated the effect of disrupting the UFMylation system on an endogenous ERAD client, core-glycosylated (CG) CD147, a ubiquitously expressed type I integral membrane protein that is constitutively degraded in a strictly HRD1-dependent manner (31). Endogenous CD147(CG) was stabilized to an extent comparable to that observed for A1AT^{NHK}-GFP and GFP-RTA^{E177Q} in a stable line of *UFM1*^{KO} K562 cells (Fig. 1*C* and *SI Appendix*, Fig. S1*C*), and in stable lines of U2OS cells defective in UFMylation or de-UFMylation (Fig. 1*D* and *SI Appendix*, Fig. S1*D*). Impaired ERAD resulting from *UFSP2* knockout in U2OS cells was rescued by reintroducing wild-type UFSP2, but not a catalytically inactive mutant (UFSP2^{C302S}) (32) or a mutant linked to Beukes hip dysplasia (UFSP2^{Y290H}), an early-onset dominantly inherited osteoarthritis (15) (Figs. 1*E* and 2*E*). By contrast, the effects of disrupting UFM1 conjugation or deconjugation on CD147(CG) turnover in HEK293 cells were far more modest (Fig. 1*F* and *SI Appendix*, Fig. S1*E*), indicating that impaired ERAD, like the ER stress phenotype arising from loss of UFMylation (21–23), is variably penetrant and cell-type specific. These incompletely penetrant phenotypes, taken together with the absence of ERAD machinery in the UFMylome (see below), the unaltered steady-state levels of HRD1 complex components upon genetic disruption of the UFM1 pathway (*SI Appendix*, Fig. S1 *B* and *C*), and the transcriptional control of UFMylation genes by the UPR (20), support the conclusion that UFMylation is required to maintain protein homeostasis in the ER by a process independent of ERAD.

Ribosomal Protein RPL26 Is a Primary Target of UFMylation. We used a stringent proteomic strategy to identify covalently UFMylated proteins in HEK293 cells (Fig. 2). Because affinity-capture proteomic analysis is highly prone to false positives resulting from nonspecific binding of abundant or "sticky" proteins (33), even when conducted under stringent denaturing conditions with bead-only or antibody controls, we exploited the fact that UFMylation is a covalent process that is strictly dependent on the activity of the UFM1-specific E1 activating enzyme, UBA5. Moreover, as a recent study reported that UFM1 conjugates are subject to efficient and constitutive deconjugation by UFSP2, resulting in exceedingly low steady-state conjugate abundance (16), we conducted UFMylome analysis in cells engineered to lack either UFMylation or de-UFMylation. To this end, we expressed a C-terminally truncated and histidine-tagged UFM1 variant, 6xHis-UFM1$^{\Delta SC}$, in cells lacking *UFM1* alone or in double knockout cells lacking *UFM1* and *UBA5* or *UFM1* and *UFSP2* (Fig. 2*A*). The use of the C-terminally truncated UFM1 bypasses the need to remove the C-terminal SerCys dipeptide from pro-UFM1 to expose the reactive C-terminal Gly (Fig. 1*A*) (6, 16). Immunoblot analysis conducted under reducing and nonreducing conditions confirmed that 6xHis-UFM1$^{\Delta SC}$ formed thioester conjugates with the UFM1-specific E2, UFC1, in otherwise wild-type (*UFM1*^{KO};6xHis-UFM1$^{\Delta SC}$) and in double knockout (*UFM1*^{KO}, *UFSP2*^{KO}) cells expressing 6xHis-UFM1$^{\Delta SC}$, but not in double knockout (*UFM1*^{KO}, *UBA5*^{KO}) cells expressing 6xHis-UFM1$^{\Delta SC}$ (*SI Appendix*, Fig. S2*A*). Importantly, while expressing 6xHis-UFM1$^{\Delta SC}$ in these lines led to ∼15-fold higher levels of monomer compared with endogenous UFM1 in wild-type HEK293 cells, the pattern and relative intensity of UFM1 conjugates was largely unaltered (*SI Appendix*, Fig. S2*B*). LC-MS/MS analysis of Ni-NTA captured proteins identified between 1,774 and 1,928 proteins in each of the three pulldown conditions, with a combined total of 2,415 unique identifications from all three conditions, including 12 proteins that had been identified in previous UFMylome analyses (Dataset S1). The fact that the total number of identifications neither decreased nor increased appreciably upon ablation of *UBA5* or *UFSP2*, respectively, suggests that the majority of captured proteins are likely to be nonspecific. Only one protein, RPL26/L1 (uL24), exhibited a substantial increase in abundance following *UFSP2* knockout (Fig. 2*B*). RPL26 is encoded by two distinct genes in eukaryotes, *RPL26* and *RPL26L1*. These genes encode paralogous proteins differing by only two amino acids, making the origins of all but two tryptic RPL26 or RPL26L1 peptides indistinguishable by mass spectrometry. Comparison of integrated ion peak intensities of peptides containing the distinguishing amino acids indicates that RPL26 is ∼15 times more abundant than RPL26L1 in UFM1-captured material, comparable to their relative abundances in RPL26 immunoblot analysis of lysates (Dataset S1). As no functional distinction between RPL26 and RPL26L1 is known and because most peptides could match to either paralog, we combined the RPL26-matched spectral counts into a single term, "RPL26/L1."

To identify other potential UFM1 conjugates, we applied three sequential filtering steps eliminating: (*i*) low confidence hits (fewer than three unique peptides in *UFSP2*^{KO}), (*ii*) proteins that failed to increase in abundance in response to knockout of *UFSP2*, and (*iii*) proteins that increased in abundance following ablation of *UBA5* (*SI Appendix*, Fig. S2*C* and Dataset S1). Notably, none of the previously reported candidates of UFMylation, including DDRGK1 (5), ASC1 (7), RPS3 (uS3), RPS20 (uS10), and RPL10 (uL16) (18), met these criteria. The 18 proteins that did survive these filters are listed in *SI Appendix*, Table S1. Although all proteins in *SI Appendix*, Table S1 conform to our minimal criteria as potential covalent UFMylation targets, most were identified with low total spectral counts (TSCs) or showed weak responses to ablation of *UBA5* and *UFSP2*. An independent biological replicate of this proteomic analysis (Dataset S1) identified RPL26/L1 as the only protein in common between the two datasets that meets our filtering criteria. Together, these data lead us to conclude that RPL26(L1) is the principal target of UFMylation in HEK293 cells.

The above proteomic results were confirmed by RPL26 and UFM1 immunoblot analyses of denatured cell lysates, which identified two RPL26 species in HEK293 cells with mobilities corresponding to adducts conjugated with one or two UFM1 moieties (Fig. 2 *C* and *D*). Both species increased in abundance upon disruption of *UFSP2* but were undetectable in *UBA5*^{KO} cells (Fig. 2*C*). Neither RPS3 nor RPS20, reported to be modified by UFM1 (18), were detected in the affinity-captured fractions. Both singly and doubly UFMylated RPL26 species were also detected in UFM1 and

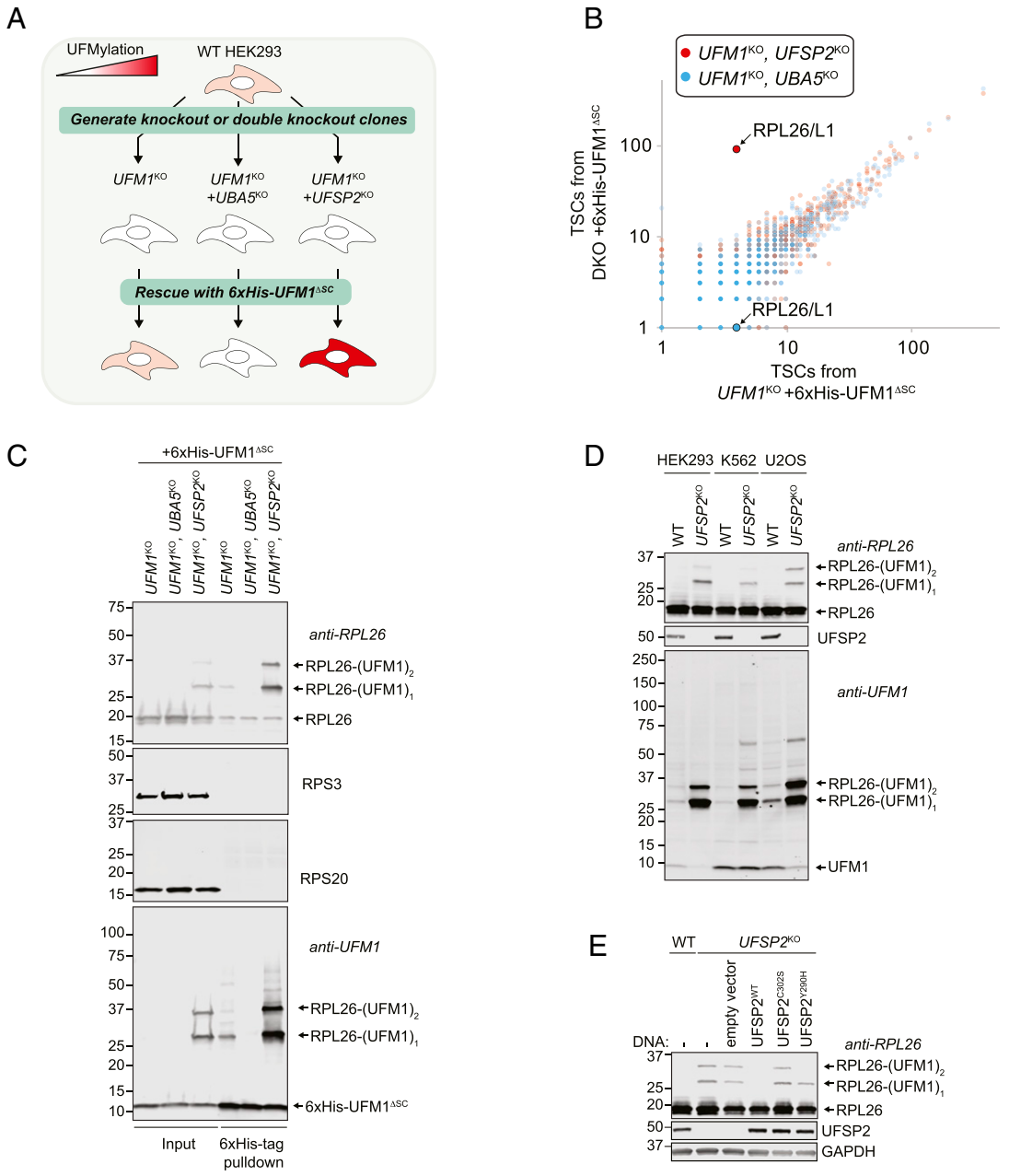

Fig. 2. RPL26 is the principal target of UFMylation. (*A*) Schematic showing the genotypes of cell lines used for proteomic analysis of the UFMylome. Extent of UFMylation is represented by red intensity. (*B*) Proteomic analysis of the UFMylome. HEK293 cells expressing 6xHis-UFM1$^{\Delta SC}$ in *UFM1*^{KO} or double knockout (DKO; *UFM1*^{KO}, *UBA5*^{KO} or *UFM1*^{KO}, *UFSP2*^{KO}) genetic backgrounds were lysed under denaturing conditions and subjected to affinity capture with Ni-NTA and LC-MS/MS analysis. TSCs for proteins identified from each affinity capture are plotted. TSCs for the nearly identical RPL26 and RPL26L1 are combined. (*C*) RPL26 UFMylation is undetectable in *UBA5*^{KO} cells and increased in *UFSP2*^{KO} cells. The indicated HEK293 cells were lysed under denaturing conditions and lysates were subjected to affinity capture with Ni-NTA. Inputs and Ni-NTA bound material were analyzed by immunoblotting with the indicated antibodies. Mobilities of mono- and di-UFMylated RPL26 are indicated. (*D*) RPL26 UFMylation is detected in different cell lines. Triton X-100 lysates of the indicated wild-type or *UFSP2*^{KO} cell lines were analyzed by immunoblotting with the indicated antibodies. The most abundant conjugates detected with a UFM1 antibody (*Bottom*) comigrate with the UFMylated species of RPL26 (*Top*). (*E*) RPL26 UFMylation is enhanced in cells expressing catalytically inactive UFSP2. Triton X-100 soluble lysates of wild-type or *UFSP2*^{KO} U2OS cells stably expressing the indicated UFSP2 construct were analyzed by immunoblotting with the indicated antibodies.

RPL26 immunoblots of K562 and U2OS cells lacking UFSP2 (Fig. 2*D*), indicating that RPL26 is also the primary target of UFMylation in cells of hematopoietic and bone lineages. UFMylated RPL26 was undetectable in wild-type U2OS cells and in *UFSP2*^{KO} U2OS cells rescued with wild type, but not catalytically inactive (C302S), UFSP2 (Fig. 2*E*), confirming a catalytic role for this protein in the UFMylation cycle. Surprisingly, only mono-UFMylated RPL26 was detected in *UFSP2*^{KO} U2OS cells expressing the human disease mutant, UFSP2^{Y290H}, suggesting that this mutation imparts a partial loss of function and that de-UFMylation of RPL26 may be a sequential process.

To identify UFMylation sites on RPL26 we used electron-transfer and higher-energy collision dissociation (EThcD) MS analysis of affinity-captured, gel-purified mono- and di-UFMylated RPL26 to identify peptides with the expected 156.09-Da mass increase arising from a Lys-GlyVal (K-GV) isopeptide remnant

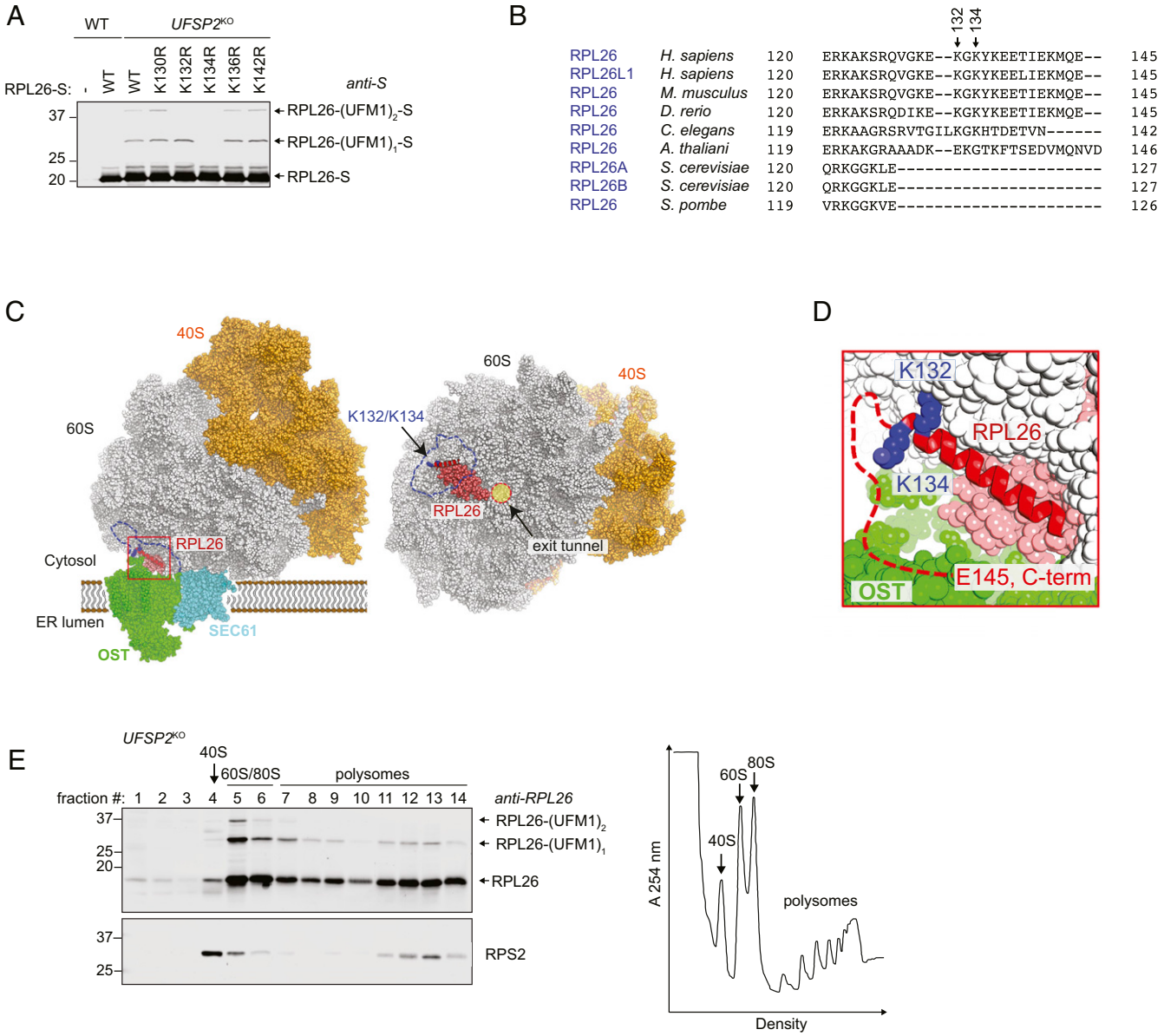

Fig. 3. RPL26 is UFMylated on K132 and K134. (*A*) The indicated RPL26-S constructs were transfected into wild-type or *UFSP2*^{KO} HEK293 cells. Cells were harvested 48 h posttransfection, lysed, and analyzed by immunoblotting with an S-tag antibody. (*B*) UFMylation sites on RPL26 are conserved in metazoans but absent in fungi. Sequence alignment of the C terminus of RPL26 from the indicated species was generated using Clustal Omega. RPL26 UFMylation sites identified by LC-MS/MS analysis are indicated with arrows. (*C*, *Left*) Model of the mammalian 80S ribosome bound to the SEC61/OST complex generated from Protein Data Bank (PDB) depositions 6FTG and 4UG0 (34, 36). (*C*, *Right*) View of the 60S ribosome exit tunnel opening (PDB 6FTG). RPL26 (red) is adjacent to the opening of the exit tunnel (yellow circle). K132 and K134 of RPL26 are colored blue. Dashed blue lines outline the approximate accessible surface area of UFM1 when conjugated to K134. (*D*) Closeup of the region encapsulated by the red box in *G* showing the location of K134 and K132 (blue) on the C-terminal helix of RPL26 (red). Dashed red line represents the flexible C terminus of RPL26, starting at Y135 and ending at E145, for which there is no density in the EM 3D reconstructions. (*E*) UFMylated RPL26 is assembled into ribosomes. Sucrose gradient sedimentation was performed on *UFSP2*^{KO} HEK293 cells using a 10–50% sucrose gradient. Collected fractions were analyzed by immunoblotting (*Left*) and A_{254} absorbance (*Right*).

generated from the C terminus of UFM1 upon ArgC digestion (*SI Appendix*, Fig. S2 *D* and *E*). High-quality EThcD spectra revealed that mono-UFMylated RPL26 contains a K-GV remnant on lysine 134 while di-UFMylated RPL26 contains K-GV on lysine 134 and on lysine 132 (*SI Appendix*, Fig. S2*F*). Immunoblot analysis of HEK293 cells expressing an S-tagged RPL26 or RPL26L1 K132R mutant lacked detectable di-UFMylated RPL26/L1-S, while the K134R mutant exhibited substantial reduction in the intensity of both mono- and di-UFMylated species (Fig. 3*A* and *SI Appendix*, Fig. S2*G*). These data confirm the MS identification of these two lysines as the sites of UFMylation and suggest that UFMylation of K134 is likely to be a prerequisite for adding a second UFM1 at K132, supporting the conclusion that RPL26 UFMylation, like de-UFMylation, may be a sequential process. CRISPR-mediated replacement of an endogenous genomic *RPL26* allele with a TAP-tagged K132R/K134R double mutant (2KR) also abolished UFMylation (*SI Appendix*, Fig. S2*H*), confirming that K132 and K134 are highly specific acceptors for UFM1 on RPL26. These sites of RPL26 UFMylation map to a C-terminal extension that is conserved in metazoans but completely absent from yeast RPL26 (Fig. 3*B*). Because the UFM1 pathway is also absent from fungi (1), these data suggest that the C-terminal extension

of RPL26 coevolved with the UFMylation pathway in the transition from unicellular to multicellular life.

RPL26 is a small, evolutionarily conserved, basic ribosomal protein, positioned on the surface of the large ribosomal subunit near RPL4 and RPL37 (Fig. 3*C* and *SI Appendix*, Fig. S3*A*) and directly adjacent to the polypeptide exit tunnel (34). The function of RPL26 in protein synthesis is obscure; yeast lacking both RPL26 paralogs exhibit mild growth defects and no apparent impairment of ribosome biogenesis or protein synthesis (35). However, RPL26's location on the ribosome and its proximity to the docking sites for SRP, the SEC61 translocon, and the oligosyl transferase (OST) complex (Fig. 3*C* and *SI Appendix*, Fig. S3*B*) (36), suggest that the UFMylation state of RPL26 could influence the interaction of ribosomes with core components of the protein translocation apparatus. The two UFMylated lysines, K132 and K134, are positioned on an α-helical extension (Fig. 3*D*) with K134 appearing more solvent exposed than K132, which is oriented toward the surface of the ribosome. This orientation is consistent with a sequential process of UFMylation wherein modification of the more accessible K134 could precede and perhaps facilitate conjugation of UFM1 to K132. Approximately 70% of UFMylated RPL26 in *UFSP2*^{KO} HEK293 cells cofractionated on sucrose density gradients with 60S subunits and 80S ribosomes and ∼30% was associated with polysome fractions, indicating that UFMylated RPL26 is incorporated into translating ribosomes (Fig. 3*E*). A similar distribution of UFMylated ribosomes was observed in wild-type cells (*SI Appendix*, Fig. S3*C*), establishing that UFMylated RPL26 is incorporated into translating ribosomes at steady state.

RPL26 Is UFMylated and De-UFMylated at the ER. UFM1 conjugation, like ubiquitin and other UBLs, is initiated in the cytosol by ATP-dependent activation of a thioester adduct to UBA5 (E1) followed by sequential transfer of UFM1 to UFC1 (E2) and ultimately, to target proteins in a reaction catalyzed by an E3 ligase complex composed of at least three proteins, UFL1 (also known as RCAD/NLBP/KIAA0776/Maxer), CDK5RAP3 (also known as LZAP), and DDRGK1 (also known as UFBP1/C20orf116) (19) (Fig. 1*A*). We observed that siRNA-mediated depletion of UFL1 or DDRGK1 from *UFSP2*^{KO} U2OS cells greatly reduced the amount of both mono- and di-UFMylated RPL26, suggesting an essential role of these two proteins in RPL26 UFMylation (Fig. 4*A*). Knockdown of UFL1 also resulted in reduced levels of DDRGK1 and CDK5RAP3, consistent with these three proteins forming an interdependent complex (19, 37). Knockdown of CDK5RAP3 caused a loss of di-UFMylated RPL26 and a concomitant increase in the mono-UFMylated species, suggesting that, while UFL1 and DDRGK1 are essential for RPL26 UFMylation at K134, CDK5RAP3 may contribute to the addition of the second UFM1 to mono-UFMylated RPL26. DDRGK1 is tethered to the ER membrane by an N-terminal signal anchor that confers a type I topology, with the bulk of its mass present in the cytoplasm (19, 24). Unsurprisingly, the UFM1 E3 ligase complex, composed of DDRGK1, UFL1, and CDK5RAP3, cofractionated with the ER in wild-type cells, but UFL1 and CDK5RAP3 redistributed to the cytosol in *DDRGK1*^{KO} cells (Fig. 4*B*), confirming the essential role of this membrane protein in recruiting the complex to the ER membrane.

Consistent with the restriction of the RPL26 UFM1 ligase complex to the ER, we found that UFMylated RPL26 was enriched in membrane fractions of *UFSP2*^{KO} cells (Fig. 4 *C* and *F*). Rescue of *DDRGK1*^{KO} cells with a mutant lacking the 28-amino acid N-terminal signal anchor (DDRGK1-S$^{\Delta TM}$) caused UFMylated RPL26 to redistribute to the cytosol (Fig. 4*D*) where it remained ribosome bound (Fig. 4*E*). Thus, localization of the UFL1/CDK5RAP3/DDRGK1 E3 complex to the ER membrane ensures that RPL26 UFMylation occurs exclusively at the ER surface. Moreover, detection of UFMylated RPL26 in the cytosol of DDRGK1-S$^{\Delta TM}$ cells, but not membrane-bound UFMylated RPL26 in wild-type cells (Fig. 4*D*) despite equivalent expression of endogenous UFSP2, suggests that efficient de-UFMylation of ER bound RPL26-UFM1 may require corestriction of substrate and de-UFMylase to the ER surface. Indeed, we observed that knocking out *ODR4*, which in *Caenorhabditis elegans* encodes a C-terminal tail-anchored ER resident protein that binds to the UFSP2 ortholog, ODR8 (38), phenocopied the effects of *UFSP2*^{KO} on ERAD substrate stabilization (Fig. 1*B*) and on RPL26 UFMylation (Fig. 4*F*), demonstrating that RPL26 de-UFMylation is also spatially restricted to the ER surface. The cytosolic localization and decreased steady-state levels of UFSP2 in *ODR4*^{KO} cells suggest that UFSP2 stability depends on its restriction to the ER surface via binding to ODR4. Together, these data suggest that a cycle of UFMylation and de-UFMylation of ribosome-assembled RPL26 occurs at the cytosolic surface of the ER, a finding supported by our ability to coprecipitate UFMylated RPL26 with antibodies to the SEC61 translocon (Fig. 4*G*). These findings suggest a direct link between the UFM1 conjugation cycle and protein biogenesis at the ER and provide a plausible explanation for the observations that defective UFMylation leads to elevated ER stress and impaired ERAD.

To formally test whether loss of RPL26 UFMylation underlies the ERAD phenotype that originally led us to investigate the UFMylation pathway, we used a gene replacement strategy to substitute for the wild-type protein, a UFMylation-resistant RPL26 variant (RPL26^{5KR}) in which all five lysines on the C-terminal α-helical domain were replaced with arginine, a mutation that does not affect its incorporation into ribosomes (*SI Appendix*, Fig. S3*D*). Because cells lacking both RPL26 and RPL26L1 exhibit a severe growth defect, we generated a cell line that constitutively expresses S-tagged RPL26 or RPL26^{5KR} and used CRISPR interference (CRISPRi) to knock down expression of endogenous RPL26 in these cells. In cells transduced with control sgRNA, endogenous RPL26 and transgenic S-tagged protein were both detectable (Fig. 4*H*). However, in cells expressing *RPL26* sgRNA, relative expression of the transgene was elevated such that the total abundance of RPL26 was constant across the cell lines, consistent with data indicating that unassembled RPL26 is efficiently degraded (39). CD147(CG) turnover in U2OS cells expressing *RPL26* sgRNA and ectopic wild-type RPL26-S was indistinguishable from turnover in wild-type U2OS cells (Fig. 4*H*, *Left*). By contrast, depletion of endogenous RPL26 led to ∼60% replacement of total RPL26 with RPL26^{5KR}-S and concomitantly pronounced impairment of CD147(CG) degradation (Fig. 4*H*, *Right*), comparable in magnitude to the effects of complete ablation of UFM1 conjugation or deconjugation. Thus, the ERAD phenotype that led us to the UFMylation pathway can be fully recapitulated by replacing endogenous RPL26 with an UFMylation-resistant variant, formally establishing the C terminus of RPL26 as the primary target of UFMylation, and linking the effects of UFM1 disruption on ER homeostasis to modification of this ribosomal protein.

Disruption of UFMylation Affects Transcription but Not Translation. Because RPL26 is a core component of the ribosome, we wondered how UFMylation might influence translation. As RPL26 is UFMylated at the ER, we performed ribosome profiling on cytosolic and ER-enriched cellular fractions and compared the translational differences in *UFM1*^{KO} and *UFSP2*^{KO} cells relative to wild-type controls, in conjunction with mRNA-seq analysis from unfractionated lysates (Fig. 5*A* and Dataset S2). Both mutants had substantial effects on the translatome of HEK293 cells. Consistent with the ER localization of the UFMylation machinery, the membrane fraction changed much more than the cytosolic fraction. Overall, these changes were driven by mRNA abundance, however, and we observed little evidence of translational disruption. Likewise, examination of individual profiles did not reveal substantial changes in ribosome footprint distribution of membrane-associated transcripts in aggregate or on individual candidate genes (Dataset S3). Taken together, these data argue against a model whereby UFMylation of RPL26 directly regulates translation of ER-associated mRNAs, and show that our

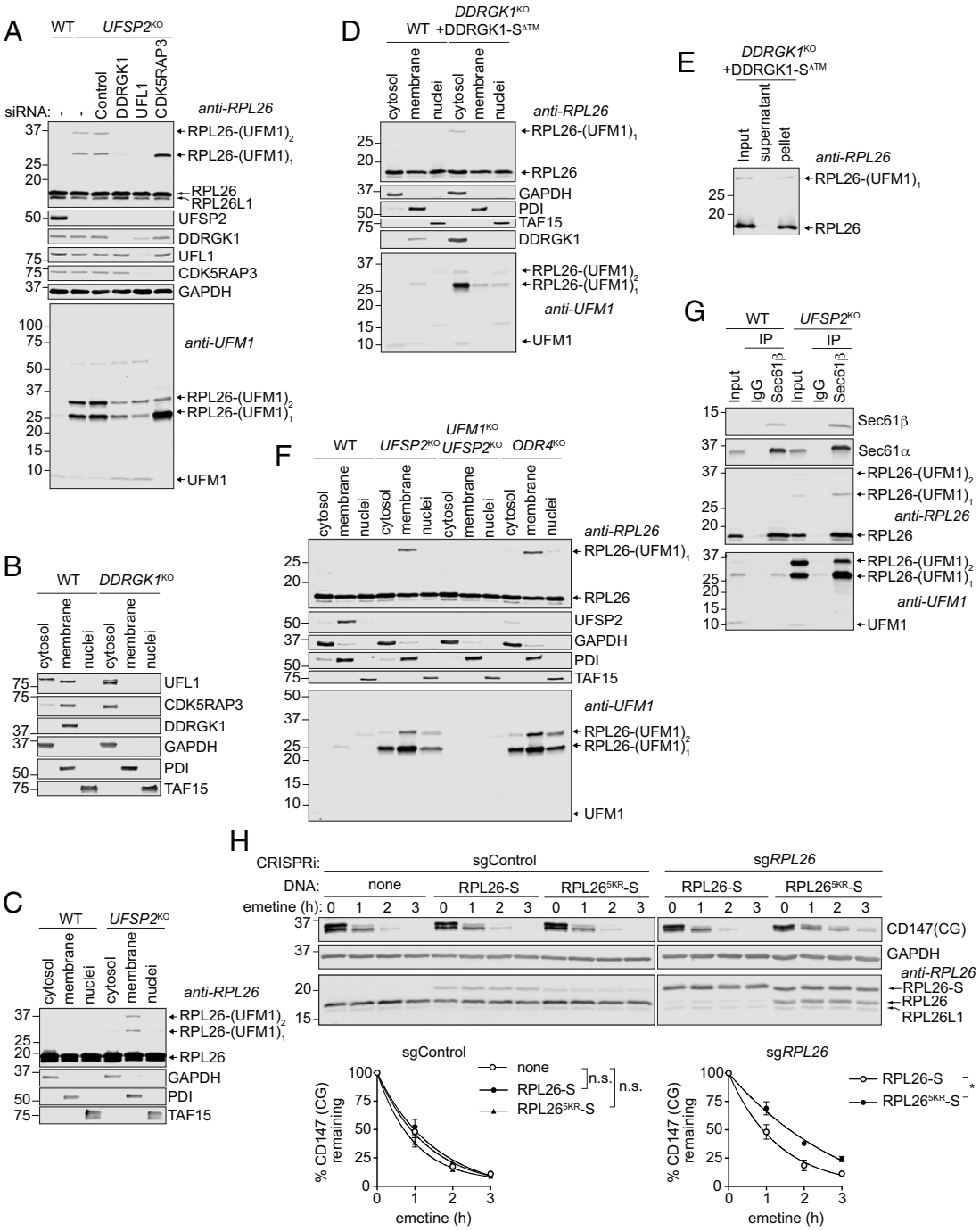

Fig. 4. RPL26 is UFMylated and de-UFMylated at the ER membrane. (*A*) Knockdown of DDRGK1, UFL1, and CDK5RAP3 diminishes RPL26 UFMylation. Wild-type or *UFSP2*^{KO} U2OS cells were untransfected (–), or transfected with the indicated siRNAs. Triton X-100 soluble lysates were analyzed by immunoblotting. UFM1 and RPL26 immunoblots were obtained by 4–15% and 12% SDS/PAGE, respectively. (*B*) DDRGK1 is required for localization of UFL1 and CDK5RAP3 to membranes. Wild-type or *DDRGK1*^{KO} U2OS cells were subjected to sequential detergent extractions to isolate crude fractions before immunoblot analysis. (*C*) UFMylated RPL26 is enriched at membranes. As in *B* except wild-type cells U2OS were compared with *UFSP2*^{KO} cells. (*D*) DDRGK1 determines the localization of UFMylated RPL26. As in *C* except wild-type HEK293 cells were compared with *DDRGK1*^{KO} cells stably expressing C-terminally S-tagged DDRGK1 lacking its predicted transmembrane domain (DDRGK1$^{\Delta TM}$-S). (*E*) Cytosolic UFMylated RPL26 assembles into ribosomes. Sucrose cushion sedimentation of lysates derived from HEK293 cells expressing only DDRGK1$^{\Delta TM}$-S. (*F*) UFMylated RPL26 is detected in the membrane fraction of *ODR4*^{KO} cells. The indicated HEK293 cells were fractionated with sequential detergent extractions before immunoblot analysis with the indicated antibodies. (*G*) UFMylated RPL26 associates with SEC61 translocons. Wild-type or *UFSP2*^{KO} U2OS cells were solubilized with buffer containing 1% DMNG and subjected to immunoprecipitation with either normal rabbit IgG or antibodies raised against Sec61β. Inputs and precipitated material were divided equally and analyzed by immunoblotting. UFM1 and RPL26 immunoblots were obtained by 4–15% and 12% SDS/PAGE, respectively. (*H*) Loss of RPL26 UFMylation impairs ERAD of CD147(CG). (*Top*) Cells were treated with emetine for the indicated times before lysis and subjected to immunoblot analysis. (*Bottom*) Quantification represented as the mean ± SEM; $n = 3$. n.s., statistically not significant, $P > 0.05$ and $^*P < 0.05$ obtained by Student's t test.

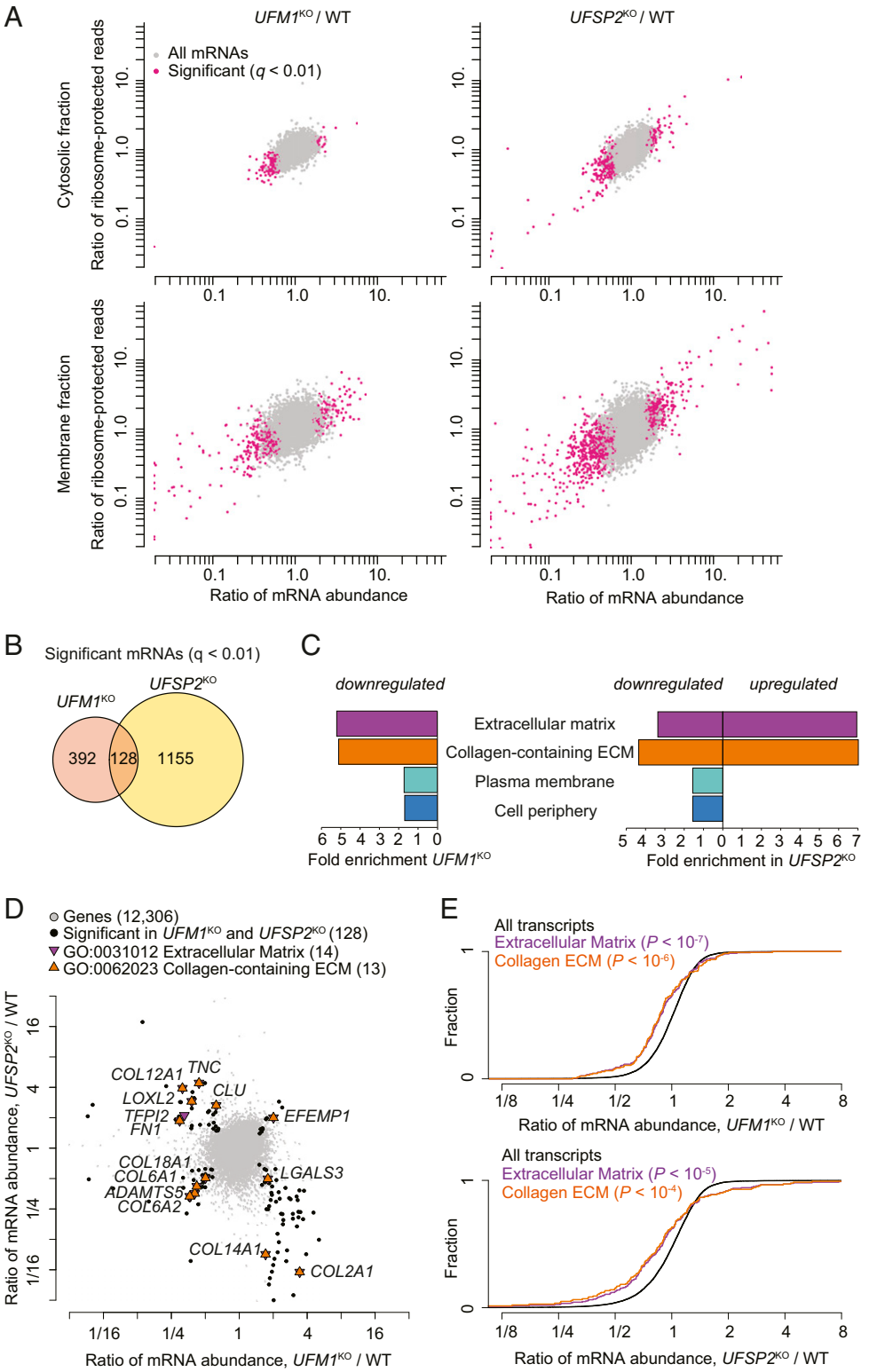

Fig. 5. Disruption of UFMylation affects transcription but not translation. (*A*) Scatterplots of the fold changes (knockout/wild type) in ribosome-protected reads in either cytosol or membrane fractions and of fold changes in RNA-seq reads from whole cell lysates. Pink dots represent genes that were statistically significant in the RNA-seq dataset only [false discovery rate (FDR) <0.01]. (*B*) Venn diagram of genes with significantly different expression (FDR <0.01) in *UFM1*^{KO} and *UFSP2*^{KO} HEK293 cells compared with wild type. (*C*) GO analysis of *UFM1*^{KO} and *UFSP2*^{KO} expression changes. Genes up-regulated or down-regulated in knockout cells were analyzed separately to identify statistically overrepresented GO terms (FDR <0.05, Fisher's exact test). GO cellular component terms shared in analysis of both knockouts are displayed. The terms "extracellular matrix" and "collagen-containing ECM" were overrepresented in both up-regulated and down-regulated genes in *UFSP2*^{KO}. (*D*) mRNA expression differences for *UFSP2*^{KO} and *UFM1*^{KO} cells versus wild type. Black circles indicate genes with significant differential expression in both mutants. Colored symbols highlight significantly changed genes in GO component categories related to the ECM. (*E*) Cumulative distribution of fold changes of genes with extracellular matrix or collagen-containing extracellular matrix annotations. *P* values were obtained by a Mann–Whitney–Wilcoxon *U* test.

profiling data reflect adaptive changes in the transcriptome that accompany the loss or constitutive gain in UFMylation.

These transcriptional changes provide some clues regarding the cellular role for RPL26 UFMylation, although they are indirect and likely adaptive effects. Broader gene expression changes were observed in *UFSP2*^{KO} cells than in *UFM1*^{KO} (Fig. 5*B* and Dataset S2), suggesting either that loss of de-UFMylation is more disruptive, or perhaps that *UFSP2* has a secondary role beyond removing UFM1 from conjugates. We also observed a stronger effect on genes identified in membrane fractions of the ribosome profiling experiment than those in the cytosolic fraction (Fig. 5*A*) consistent with the localization of the UFMylation and de-UFMylation machinery to the ER. The intersection of gene ontology (GO) terms associated with significantly up-regulated and down-regulated transcripts in *UFM1*^{KO} and in *UFSP2*^{KO} RNA-seq revealed a significant enrichment of transcripts encoding extracellular matrix (ECM) proteins, particularly those comprising the collagen-containing ECM (Fig. 5 *B–E* and Dataset S4). While the ECM GO term was enriched in the down-regulated *UFM1*^{KO} gene list, the ECM GO term was enriched in both up-regulated and down-regulated gene lists for *UFSP2*^{KO}, suggesting that constitutive UFMylation has opposing effects on different subsets of ECM genes.

Discussion

Our results establish that RPL26, a largely uncharacterized ribosomal protein, is the principal cellular target of UFMylation and suggest that this covalent modification directly contributes to cotranslational protein translocation into the ER, providing a functional link between UFMylation and ER protein homeostasis. Other proteins, including different ribosomal subunits (18), have been previously proposed to be UFMylation targets. Although some of these were identified in our UFM1-captured proteomes, none survived stringent filtering and dataset replication. Moreover, among the reported UFM1 targets, only two, DDRGK1 (5) and ASC1 (7), have been shown to depend on UFM1 conjugating machinery. DDRGK1, the membrane anchor for the UFM1 E3 ligase complex, previously identified only following overexpression (5), was not identified in our UFMylome. Like the E3s for ubiquitin and other UBLs, DDRGK1 is subject to automodification by UFM1 when overexpressed (5, 16). ASC1, a nuclear receptor coactivator reported to be a covalent UFMylation target (7), was also absent from our replicate datasets and has not been independently validated. The finding that UFM1 and UFM1 conjugation genes are transcriptional targets of the UPR (20) has suggested a link to the secretory pathway, but a mechanistic connection between these processes has been elusive. Moreover, the relatively modest effect sizes and incompletely penetrant phenotypes of UFM1 disruption on UPR activation (22, 23) and ERAD impairment (Fig. 1) suggest that these homeostatic processes are not directly controlled by UFMylation but instead are respones to an elevated burden of malfolded or misassembled proteins within the ER lumen in the absence of a functional UFMylation system.

Our data suggest that the ERAD phenotype that originally led us to the UFMylation pathway is an indirect consequence of aberrant protein biogenesis in the ER caused by disrupted UFMylation or de-UFMylation. Mammalian cells contain several ERAD modules specialized to handle different topological classes of folding- or assembly-defective proteins (40). The HRD1 module is responsible for dislocating and ubiquitylating luminal proteins like A1AT^{NHK} and RTA, as well as integral membrane proteins like CD147 that have most of their mass inside the ER (28, 31). Our observation of preferential stabilization of these HRD1 clients over the GP78 substrate, INSIG1, together with the lack of effect on the cytosolic ERAD client, GFP^{u}*, in cells lacking UFMylation, suggests that defective biosynthetic products in UFMylation-ablated cells are likely to be enriched in proteins that are normally translocated into the ER lumen where they could compete with other HRD1 clients, including CD147(CG) and the reporters used in our genome-wide CRISPR analysis (26).

Because our RNA-seq analysis was performed on stable cell lines that constitutively lack functional UFMylation or de-UFMylation pathways, the altered gene expression profile observed in these cells likely reflects secondary adaptive changes which compensate for a primary biogenesis defect in a subset of secretory proteins. The strong overrepresentation of ECM-associated genes in this adaptive response suggests the possibility that UFMylation may contribute to correct biosynthesis of one or more ECM components. Evolution of the ECM was a key event in the transition from unicellular to multicellular life (41). The observation that UFMylation occurs on a metazoan-specific C-terminal extension of RPL26 suggests that this appendage likely also coevolved with emergence of the UFM1 system and the ECM. ECM proteins, particularly collagens, require an extensive set of specialized factors to fold, modify, assemble, secrete, process, and cross-link these large, rigid molecules (42). The robust association of human UFMylation genes with abnormal brain development and microcephaly in humans (3, 11, 23, 43) and with defective neuromuscular junction formation in *Drosophila* (12) suggests a role for UFMylation in tissue development, a process that is intimately dependent on cell–cell and cell–matrix interaction. In this regard, it is especially noteworthy that rare allelic variants of *DDRGK1* (13) and *UFSP2* (14, 15) are linked to human skeletal dysplasias affecting cartilage development and that DDRGK1 deficiency is associated with impaired cartilage development in zebrafish and with delayed chondrogenesis in the mouse (13).

Although further study is clearly required to elucidate the mechanistic relationship between UFMylation and tissue development and morphogenesis, our identification of RPL26 as the primary target of UFMylation, together with the physical proximity of UFM1-modified ribosomes to the machinery required for cotranslational protein translocation at the ER, points to a role for this ubiquitin-like modifier in the early steps of secretory protein biogenesis.

Materials and Methods

SI Appendix, Supporting Materials and Methods provides information on DNA constructs, cell culture conditions, immunoblotting, CRISPRi, emetine chase assays, endogenous RPL26 tagging, sucrose cushion sedimentation, polysome profiling, SEC61 immunoprecipitation, denaturing 6xHis-tag affinity capture, mass spectrometry and data analysis, RNA-seq analysis, ribosome profiling analysis, and GO analysis.

Knockout Cell Line Generation. sgRNA sequences used in this study are listed in Dataset S5. Gene knockouts in K562 cells with doxycycline-inducible ERAD reporters and stable expression of Cas9 were generated by introducing individual sgRNAs by lentivirus infection. Clonal K562 cells with *UFM1*^{KO} or *UFSP2*^{KO} were obtained by selecting with 0.8 μg/mL puromycin, performing limiting dilution cloning, and screening individual clones by immunoblot analysis.

Gene knockouts in HEK293 and U2OS cells were generated as reported previously (44). Briefly, cells were cotransfected with two plasmids, one expressing both Cas9 and sgRNA (pX330-U6-Chimeric_BB-CBh-hSPCas9, Addgene plasmid 42230) and the other, called pDONOR-STOP, for homology directed repair (HDR)-mediated insertion of tandem stop codons and selection with puromycin or G418. After selecting for 1–2 wk, clones were isolated by limiting dilution and screened for knockout by immunoblot analysis. Double knockouts were generated by simultaneous transfection of vectors for both target genes and combined selection with puromycin and G418.

CRISPRi of *RPL26* in U2OS Cells. U2OS cells were transfected with plasmids expressing wild-type or 5KR (K130R, K132R, K134R, K136R, K142R) RPL26. Stable pools were selected with G418 and transduced with pMCB584 (a gift from M. Bassik, Stanford University, Stanford, CA) for expression of dCas9-KRAB and BFP. BFP^{+} infected cells were enriched by sorting twice on an Aria II (BD Biosciences) cell sorter equipped with a 405-nm laser. Control sgRNA (GCCGCAATGTTTCTCATCGG) or sgRNA targeting endogenous *RPL26* (GCCATCACCGAAGCGGGAGC) were introduced by lentiviral transduction with the pMCB320 vector carrying puromycin resistance. Four days after infection, cells were selected with puromycin for 3 to 4 d. Cells were then used for emetine chase assays within 10 passages.

Emetine Chase Assays. Wild-type or knockout U2OS or HEK293 cells were grown for up to 48 h to 80–90% confluency and K562 cells were grown to a density of 0.5–1 × 10^6 cells per milliliter. Cells were left untreated (0-h time point) or treated with 10 μM emetine for the indicated times before collection in cold PBS. Cells were pelleted at 1,000 × *g*, lysed for 10 min on ice in 1% Triton X-100, 50 mM Hepes pH 7.5, 150 mM NaCl, and 1× protease inhibitor mixture (Roche), and lysates were cleared by centrifugation at 21,130 × *g*. Protein concentration was measured using a BCA Protein Assay Kit (Thermo Fisher Scientific) and adjusted to equal concentrations before SDS/PAGE and immunoblotting. Approximately 5 μg of protein was analyzed for detection of CD147(CG) and GAPDH. Band intensities were quantified using Image Studio Lite software (Li-COR Biosciences). Protein remaining was calculated as a percentage of untreated, normalized to GAPDH, and one-phase exponential decay curves were fit using Prism 7 (GraphPad Software). *P* values were obtained by a Student's *t* test applied to the slopes from each replicate, generated from log transformed data fit with linear regression.

For analysis of GFP-tagged ERAD reporter turnover, expression was induced in clonal K562 lines with doxycycline (Sigma-Aldrich) using 0.075 μg/mL for $A1AT^{NHK}$-GFP or 1 μg/mL for GFP-RTA^{E177Q} for 16 h. Cells were treated with 20 μM emetine for the indicated times and collected by centrifuging at 1,000 × *g* for 5 min, resuspended in PBS, and placed on ice. At least 20,000 events per sample were analyzed on an LSR II flow cytometer (BD Biosciences) equipped with 405, 488, and 532 lasers or on a FACSCalibur (BD Biosciences) equipped with a 488 laser. Data were analyzed using FlowJo version 10.0.8 (Tree Star).

Cell Fractionation by Sequential Detergent Extraction. HEK293 or U2OS cells were collected in PBS and pelleted by centrifuging at 1,000 × *g*. Cell pellets (~2 × 10^6) were resuspended in 200 μL of 0.02% digitonin, 50 mM Hepes pH 7.5, 150 mM NaCl, 2 mM $CaCl_2$, and protease inhibitor mixture and incubated on ice for 10 min, followed by centrifugation at 21,130 × *g* at 4 °C for 10 min. The supernatant containing cytosol was collected and the pellet was washed with 1 mL PBS before resuspending in 200 μL of 1% Triton X-100, 50 mM Hepes pH 7.5, 150 mM NaCl, and protease inhibitor mixture. After incubating for 10 min on ice and centrifuging at 21,130 × *g* at 4 °C for 10 min, the supernatant containing the membrane fraction was collected. The remaining nuclear pellet was solubilized by sonicating in 200 μL of 1% SDS, 25 mM Tris pH 8, 150 mM NaCl, 2.5 mM EDTA, and protease inhibitor mixture. Equal volumes of the collected fractions were analyzed by SDS/PAGE and immunoblotting.

ACKNOWLEDGMENTS. We thank James Olzmann, Alexey Petrov, Alex Johnson, and Joseph Puglisi for stimulating discussions and technical assistance; and Peter Sarnow for help with polysome profiling. This work was supported by Grant R01GM074874 from the National Institute of General Medical Sciences and a generous gift from the Becker Family Foundation (to R.R.K.). RNA-seq analysis was performed at the Vincent J. Coates Genomics Sequencing Laboratory at University of California, Berkeley, supported by NIH Instrumentation Grant S10 OD018174. D.E.L. was supported by postdoctoral fellowships from the NIH (F32GM113370) and the Alpha-1 foundation. C.P.W. was supported by postdoctoral fellowships from the NIH (F32GM113378) and Cystic Fibrosis Research, Inc. N.T.I. is supported by NIH Award DP2CA195768. C.R. is supported by the Shuri and Kay Curci Foundation and Graduate Research Fellowship DGW 1752814 from the National Science Foundation.

1. Komatsu M, et al. (2004) A novel protein-conjugating system for Ufm1, a ubiquitin-fold modifier. *EMBO J* 23:1977–1986.
2. Cai Y, Singh N, Li H (2016) Essential role of Ufm1 conjugation in the hematopoietic system. *Exp Hematol* 44:442–446.
3. Hamilton EMC, et al.; Recessive H-ABC Research Group (2017) *UFM1* founder mutation in the Roma population causes recessive variant of H-ABC. *Neurology* 89: 1821–1828.
4. Daniel J, Liebau E (2014) The ufm1 cascade. *Cells* 3:627–638.
5. Tatsumi K, et al. (2010) A novel type of E3 ligase for the Ufm1 conjugation system. *J Biol Chem* 285:5417–5427.
6. Kang SH, et al. (2007) Two novel ubiquitin-fold modifier 1 (Ufm1)-specific proteases, UfSP1 and UfSP2. *J Biol Chem* 282:5256–5262.
7. Yoo HM, et al. (2014) Modification of ASC1 by UFM1 is crucial for ERα transactivation and breast cancer development. *Mol Cell* 56:261–274.
8. Tatsumi K, et al. (2011) The Ufm1-activating enzyme Uba5 is indispensable for erythroid differentiation in mice. *Nat Commun* 2:181.
9. Cai Y, et al. (2015) UFBP1, a key component of the Ufm1 conjugation system, is essential for ufmylation-mediated regulation of erythroid development. *PLoS Genet* 11: e1005643.
10. Zhang M, et al. (2015) RCAD/Ufl1, a Ufm1 E3 ligase, is essential for hematopoietic stem cell function and murine hematopoiesis. *Cell Death Differ* 22:1922–1934.
11. Muona M, et al.; DDD Study (2016) Biallelic variants in UBA5 link dysfunctional UFM1 ubiquitin-like modifier pathway to severe infantile-onset encephalopathy. *Am J Hum Genet* 99:683–694.
12. Duan R, et al. (2016) UBA5 mutations cause a new form of autosomal recessive cerebellar ataxia. *PLoS One* 11:e0149039.
13. Egunsola AT, et al. (2017) Loss of DDRGK1 modulates SOX9 ubiquitination in spondyloepimetaphyseal dysplasia. *J Clin Invest* 127:1475–1484.
14. Di Rocco M, et al. (2018) Novel spondyloepimetaphyseal dysplasia due to UFSP2 gene mutation. *Clin Genet* 93:671–674.
15. Watson CM, et al. (2015) Identification of a mutation in the ubiquitin-fold modifier 1-specific peptidase 2 gene, UFSP2, in an extended South African family with Beukes hip dysplasia. *S Afr Med J* 105:558–563.
16. Ishimura R, et al. (2017) A novel approach to assess the ubiquitin-fold modifier 1-system in cells. *FEBS Lett* 591:196–204.
17. Pirone L, et al. (2017) A comprehensive platform for the analysis of ubiquitin-like protein modifications using in vivo biotinylation. *Sci Rep* 7:40756.
18. Simsek D, et al. (2017) The mammalian ribo-interactome reveals ribosome functional diversity and heterogeneity. *Cell* 169:1051–1065.e18.
19. Wu J, Lei G, Mei M, Tang Y, Li H (2010) A novel C53/LZAP-interacting protein regulates stability of C53/LZAP and DDRGK domain-containing Protein 1 (DDRGK1) and modulates NF-kappaB signaling. *J Biol Chem* 285:15126–15136.
20. Zhang Y, Zhang M, Wu J, Lei G, Li H (2012) Transcriptional regulation of the Ufm1 conjugation system in response to disturbance of the endoplasmic reticulum homeostasis and inhibition of vesicle trafficking. *PLoS One* 7:e48587.
21. Adamson B, et al. (2016) A multiplexed single-cell CRISPR screening platform enables systematic dissection of the unfolded protein response. *Cell* 167:1867–1882.e21.
22. DeJesus R, et al. (2016) Functional CRISPR screening identifies the ufmylation pathway as a regulator of SQSTM1/p62. *eLife* 5:e17290.
23. Nahorski MS, et al. (2018) Biallelic UFM1 and UFC1 mutations expand the essential role of ufmylation in brain development. *Brain* 141:1934–1945.
24. Lemaire K, et al. (2011) Ubiquitin fold modifier 1 (UFM1) and its target UFBP1 protect pancreatic beta cells from ER stress-induced apoptosis. *PLoS One* 6:e18517.
25. Li J, et al. (2018) Ufm1-specific ligase Ufl1 regulates endoplasmic reticulum homeostasis and protects against heart failure. *Circ Heart Fail* 11:e004917.
26. Leto DE, et al. (2018) Genome-wide CRISPR analysis identifies substrate-specific conjugation modules in ER-associated degradation. *Mol Cell*, 10.1016/j.molcel.2018.11.015.
27. Olzmann JA, Kopito RR, Christianson JC (2013) The mammalian endoplasmic reticulum-associated degradation system. *Cold Spring Harb Perspect Biol* 5:a013185.
28. Christianson JC, Shaler TA, Tyler RE, Kopito RR (2008) OS-9 and GRP94 deliver mutant alpha1-antitrypsin to the Hrd1-SEL1L ubiquitin ligase complex for ERAD. *Nat Cell Biol* 10:272–282.
29. Stefanovic-Barrett S, et al. (2018) MARCH6 and TRC8 facilitate the quality control of cytosolic and tail-anchored proteins. *EMBO Rep* 19:e45603.
30. Lee JN, Song B, DeBose-Boyd RA, Ye J (2006) Sterol-regulated degradation of Insig-1 mediated by the membrane-bound ubiquitin ligase gp78. *J Biol Chem* 281: 39308–39315.
31. Tyler RE, et al. (2012) Unassembled CD147 is an endogenous endoplasmic reticulum-associated degradation substrate. *Mol Biol Cell* 23:4668–4678.
32. Ha BH, et al. (2011) Structure of ubiquitin-fold modifier 1-specific protease UfSP2. *J Biol Chem* 286:10248–10257.
33. Mellacheruvu D, et al. (2013) The CRAPome: A contaminant repository for affinity purification-mass spectrometry data. *Nat Methods* 10:730–736.
34. Khatter H, Myasnikov AG, Natchiar SK, Klaholz BP (2015) Structure of the human 80S ribosome. *Nature* 520:640–645.
35. Babiano R, Gamalinda M, Woolford JL, Jr, de la Cruz J (2012) Saccharomyces cerevisiae ribosomal protein L26 is not essential for ribosome assembly and function. *Mol Cell Biol* 32:3228–3241.
36. Braunger K, et al. (2018) Structural basis for coupling protein transport and N-glycosylation at the mammalian endoplasmic reticulum. *Science* 360:215–219.
37. Kwon J, et al. (2010) A novel LZAP-binding protein, NLBP, inhibits cell invasion. *J Biol Chem* 285:12232–12240.
38. Chen C, Itakura E, Weber KP, Hegde RS, de Bono M (2014) An ER complex of ODR-4 and ODR-8/Ufm1 specific protease 2 promotes GPCR maturation by a Ufm1-independent mechanism. *PLoS Genet* 10:e1004082.
39. Sung MK, et al. (2016) A conserved quality-control pathway that mediates degradation of unassembled ribosomal proteins. *eLife* 5:e19105.
40. Christianson JC, et al. (2011) Defining human ERAD networks through an integrative mapping strategy. *Nat Cell Biol* 14:93–105.
41. Ozbek S, Balasubramanian PG, Chiquet-Ehrismann R, Tucker RP, Adams JC (2010) The evolution of extracellular matrix. *Mol Biol Cell* 21:4300–4305.
42. Ishikawa Y, Bächinger HP (2013) A molecular ensemble in the rER for procollagen maturation. *Biochim Biophys Acta* 1833:2479–2491.
43. Colin E, et al.; FREX Consortium (2016) Biallelic variants in UBA5 reveal that disruption of the UFM1 cascade can result in early-onset encephalopathy. *Am J Hum Genet* 99:695–703.
44. van der Goot AT, Pearce MMP, Leto DE, Shaler TA, Kopito RR (2018) Redundant and antagonistic roles of XTP3B and OS9 in decoding glycan and non-glycan degrons in ER-associated degradation. *Mol Cell* 70:516–530.e6.